HHS Public Access

Author manuscript

Nat Struct Mol Biol. Author manuscript; available in PMC 2015 June 01.

Published in final edited form as:

Nat Struct Mol Biol. 2014 December ; 21(12): 1075–1081. doi:10.1038/nsmb.2907.

CryoEM reveals different coronin binding modes for ADP- and ADP-BeFx- actin filaments

Peng Ge[1,2,*], **Zeynep A. Oztug Durer**[3,*], **Dmitri Kudryashov**[4], **Z. Hong Zhou**[1,2,5], and **Emil Reisler**[3,5]

[1]Department of Microbiology, Immunology and Molecular Genetics, University of California, Los Angeles (UCLA), Los Angeles, California, USA

[2]California NanoSystems Institute (CNSI), UCLA, Los Angeles, California, USA

[3]Department of Chemistry and Biochemistry, UCLA, Los Angeles, California, USA

[4]Department of Chemistry and Biochemistry, The Ohio State University, Columbus, Ohio, USA

[5]Molecular Biology Institute, UCLA, Los Angeles, California, USA

Abstract

Essential cellular processes involving the actin cytoskeleton are regulated by auxiliary proteins which can sense the nucleotide state of actin. Here we report cryo electron microscopy (cryoEM) structures at 8.6 Å resolution for ADP- and ADP-BeFx- (mimicking ADP-Pi) bound actin filaments in complex with the β-propeller domain (residues 1–600) of yeast coronin 1 (crn1). Our structures identify the main differences in the interaction of coronin with the two nucleotide states of F-actin. We derived pseudo-atomic models by fitting the atomic structures of actin and coronin into these structures. The identified binding interfaces on actin were confirmed by chemical crosslinking, fluorescence spectroscopy and actin mutagenesis. Importantly, the structures of actin and coronin mapped in this study offer a structural explanation for the nucleotide-dependent effects of coronin on cofilin-assisted remodeling of F-actin.

Introduction

Dynamic remodeling of the actin cytoskeleton by actin binding proteins is critical to many biological processes, including endocytosis, cell motility, and cell division. This remodeling is linked to actin filament age via a nucleotide-related clock. Actin filaments are distinctively different in their ATP and ADP states. ADP-bound “older” filaments (in which P_i has been released following ATP hydrolysis) were reported to be less stable[1] and to have

Corresponding author: Emil Reisler. reisler@mbi.ucla.edu.

*These authors contributed equally to this work.

Accession codes. The cryoEM maps of the ADP- and ADP-BeFx-F-actin-coronin complexes have been deposited in the Electron Microscopy Data Bank under codes EMD-6100 and EMD-6101, respectively.

Author contributions: P.G., Z.A.O.D., D.K., and E.R. designed experiments; P.G., Z.A.O.D., D.K., collected EM data; P.G. and Z.H.Z. processed, analyzed and interpreted EM data; Z.A.O.D. collected and analyzed biochemical data; all authors wrote and reviewed the manuscript.

more internal flexibility[2,3] relative to ATP- and ADP-Pi filaments. In particular, the lower stability ADP-actin filaments have a higher dissociation rate constant at the barbed ends than either ATP- or ADP-Pi filaments and lower association rate constants at both ends compared to ATP-actin filaments[4]. Biochemical evidence suggests that structural changes in subdomain 2 of ADP-F-actin are correlated with its lower stability[5,6].

Cellular remodeling of actin structures includes, among other processes, filaments severing, depolymerization, and polymerization. The ADF and cofilin protein family is the main factor involved in actin filaments severing[7,8] and exhibits a strong preference for older – the ADP state - filament segments. Cofilin severs F-actin more efficiently at sub-saturating concentrations[8] at the boundaries between bare and decorated filament regions[9]. The Arp2/3 complex, a frequent partner of ADF and cofilin in rapid reorganization of actin structures at the edge of the cell, stimulates new actin polymerization in branches radiating from the sides of existing filaments. The branch segments appear to be more stable in the ATP or ADP-Pi state of filaments[10,11]. However, despite functionally important differences in affinities of some actin binding proteins (ABPs) for the ATP, ADP-Pi, and ADP states of actin, such binding differences have not yet been examined by detailed structural analysis.

Nucleotide states of F-actin impact the binding of ABPs, which regulate the function of ADF and cofilin, and/or Arp2/3 complex. The coronin family of proteins is a prime example of such cellular complexity. Coronins are broadly expressed in eukaryotic organisms[12,13] and can bind Arp2/3 complex to impact branching of newly formed filaments[14–16]. They can also accelerate the severing of ADP-F-actin (but not ATP-F-actin) by cofilin[17]. Thus, coronins are considered to be important indirect regulators of actin dynamics in cell motility, endocytosis, and phagocytosis[12]. Their malfunction in mice and humans is linked to immunodeficiency diseases[18–20].

Among the seven mammalian coronins, coronins1–6 are highly homologous. They contain a well conserved N-terminal segment followed by WD repeats arranged into a 7-bladed β-propeller structure, a unique region, and the C-terminal coiled-coil (CC) domain[21,22]. Most of the functional studies have been done with type 1 coronins (1A, 1B, 1C), which include the yeast coronin, Crn1p. Both mammalian Coronin 1B[14] and yeast Crn1p[23] have higher affinity towards ATP-F-actin than for ADP-F-actin. In yeast, Crn1p was reported to have a genetic and functional interaction with cofilin[17,23]. As indicated above, coronin inhibits cofilin-mediated severing of ATP-actin, but promotes the severing of ADP-F-actin by cofilin[17].

As a first step toward understanding the molecular mechanism of coronin-cofilin effects on ATP-actin and ADP-actin filaments, we set out to obtain a structural description of the cofilin-actin and coronin-actin systems. A high resolution (9 Å) cryo-electon microscopy (cryoEM) structure of the cofilin-actin complex was recently reported[24]. Here, we applied helical reconstruction of cryoEM images to solve two structures: coronin-decorated ADP-F-actin and ADP-BeFx-F-actin (a structural analog of ADP-Pi-F-actin). We observed two different modes of interaction between coronin and F-actin depending on actin's nucleotide state. We obtained pseudo-atomic models of F-actin-coronin complexes by docking atomic models of individual subunits into these two structures. These models led us to predict the

interactions of the two proteins at residue level details. We provided independent experimental validation of these findings using structure-based mutagenesis, chemical crosslinking methods, and fluorescence measurements. Our results provided structural evidence for differential recognition of F-actin nucleotide states by one of its cellular binding partners. Furthermore, they suggested a mechanism for coronin's regulatory effects on remodeling of F-actin by cofilin and/or Arp2/3 complex.

Results

Coronin-bound ADP-F-actin and ADP-BeFx-F-actin structures

We observed in cryoEM images that full length Crn1p generated arrays of actin filaments (Supplementary Fig. 1), which were too dense for analysis by single particle reconstruction methods. Consequently, we used a coronin construct (Crn1ΔCC; residues 1–600) lacking the coiled-coil domain that is responsible for coronin oligomerization and actin bundling[23]. Class-average images of filament segments of these two complexes decorated with either full length coronin or Crn1ΔCC were indistinguishable by two-dimensional classification-averaging analysis. Crn1ΔCC was also shown previously to function similarly to the full length protein and synergize with cofilin both in the *in vitro* and *in vivo* assays[25]. Therefore, we chose to pursue our structural analysis of coronin bound F-actin using Crn1ΔCC.

Crn1ΔCC extensively decorated both ADP- and ADP-BeFx F-actin (Fig. 1 and Supplementary Fig. 2) at a 3:1 – 4:1 molar ratio of coronin to actin (set at 2μM). At higher molar ratios the background density of unbound coronin was limiting for structural analysis. In our images, the electron densities of coronin had a lower intensity than those of actin subunits, indicating that the decoration occupancy was probably less than 1:1 (coronin:actin). Alternatively, this lower density could result from the variable twist of F-actin, which has a stronger blurring effect at higher radius densities.

The resolutions of coronin decorated ADP-F-actin and ADP-BeFx-F-actin structures are both 8.6 Å, as determined by the "Gold-standard" 0.143 Fourier shell correlation (FSC) criteria. At this resolution, every α-helix and some β-sheets of the actin subunits can be identified in the map (Fig.1), and every β-sheet from the 7-bladed propeller of coronin can be visualized. Overall, actin subunits from both the ADP- and ADP-BeFx- states resemble closely the previously determined F-actin structures[26,27]. The two actin nucleotide states have helical symmetries of 165.9° and 166.3° per subunit for ADP- and ADP-BeFx-F-actin, respectively (as reported from the customized Relion program, see Methods). Actin subunits are similar in both states, with nearly all secondary structure elements superimposable (Fig. 1d and 1h).

Coronin footprint on ADP-F-actin and ADP-BeFx-F-actin

We obtained pseudo-atomic models for the two nucleotide states of the actin-coronin complex by fitting the atomic model of F-actin[26] (per subunit) and the yeast homology model of murine coronin crystal structure[21] into our cryoEM density maps. Both models can be unambiguously docked into their corresponding densities in both states (Fig. 1c,d,g,h). [For the pseudo symmetry of coronin, only one out of seven possible dockings is

significantly favored, as indicated by the docking scores (Supplementary Fig. 3).] Coronin-actin interaction sites identified by this docking agree with the binding effects of actin mutagenesis reported below. They are also consistent with the loss of affinity for actin of coronin mutants[25] Crn1-2 (K10A R12A), Crn1-6 (R141A K142A), Crn1-13 (K295A D297A), Crn1-17(E320A R323A), and Crn1-19 (R361A R362A E364A E365A). These indicated coronin residues and the critical actin residues identified by our mutagenesis experiments (below) are located at the coronin-actin interface suggested by our pseudo-atomic models, thus validating these models.

In models for both nucleotide states, the common contacts of coronin were to subdomains 1 and 2 of “i” actin and subdomain 1 of “i+2” actin i.e., the consecutive subunit along the same filament strand (Figs. 2–3, and Supplementary Video 1, details discussed in the next section). However, the interaction of coronin with the opposite strand of the filament differed notably between the two states. In ADP-F-actin we observed that coronin straddled the two filament strands by making extensive contacts to the opposite strand (through subdomains 3 and 4 of its “i+1” actin and subdomain 4 of its “i−1” actin) (Fig. 2a). This interaction may involve charge complementarity between “i+1” actin’s residues Asp222, Lys315 and Glu316 and their respective pairs on coronin, Lys20, Glu22 and Lys21 (Fig. 2a). In contrast, coronin contacts to the other strand are weak in the ADP-BeFx state[28,29] [mimicking the ADP-Pi state of the filament[30]], and involve only slightly subdomain 4 of the “i+1” actin (Fig. 2b). One likely charge interaction in this state could be between Lys21 and Lys69 of coronin and Glu224 on subdomain 4 of “i+1” actin. These residues are close together and could interact by charge complementarity when in favorable rotamers (Fig. 2b).

The difference between the two binding modes of coronin can be explained as a rotation by approximately 20° around an axis passing through residues Asp183, Arg202, and Lys227 of coronin (Fig. 2a and Supplementary Video 1). As a result of this rotation, the interface of coronin with subdomain 1 of actin subunit “i" in both ADP- and ADP-P_i states was largely preserved. On the other hand, distant contacts with actin subunit “i+2” and, in particular, contacts with the opposite strand were affected substantially (Supplementary Video 1).

Another difference between the two nucleotide state structures appears in the interaction of coronin with subdomain 1 of actin subunit “i+2” (Fig. 2). In our model of the ADP state, the C-terminal loop of actin (residues 371–375) faces a hydrophobic environment on coronin composed of His13, Phe15, Phe358 and Pro360 (Fig. 2c). In contrast, our model of the ADP-BeFx state shows that the same actin loop faces a polar environment on coronin, composed of residues 17–22 (Gln17, Lys20, Lys21, and Glu22) (Fig. 2d). To test this, we attached a small fluorescent probe, acrylodan, to actin’s C-terminal Cys374. Consistent with our models, coronin binding caused a larger blue-shift in the spectrum of acrylodan-ADP-F-actin than acrylodan-ADP-BeFx-actin (Fig. 2e,f), supporting its greater burial in a hydrophobic environment in the ADP-F-actin. Notably, binding of several other ABPs to actin was also shown to be modulated by conformational changes in actin’s C-terminal region[31–33].

Ionic interactions govern coronin binding to F-actin

Pseudo-atomic models of the actin-coronin complexes suggest that major interactions between coronin and F-actin are predominantly electrostatic and similar in both nucleotide states. Indeed, an increase in the buffer ionic strength (from 50 mM to 150 mM KCl) decreased coronin-actin binding affinity by two-fold (Table 1). The proposed interface between coronin and actin shows good charge and shape complementarity. Actin “i”, which has the greatest contact area with coronin (Fig. 3a), has extensive electrostatic interactions with a prominent positively charged “corridor” on the “top” surface of the coronin’s beta propeller domain (Fig. 4). The charged “corridor” on coronin is composed of lysines 204, 227 and 247 and an arginine (residue 323). These three lysines interact synergistically and respectively with Glu99, Glu83, and Glu100 on actin “i" (Fig. 3d). In our model, Arg323 is in the proximity (4–6 Å) of actin’s Asp80-Asp81 acidic patch. These putative ionic interactions with coronin span the entire actin helix 78–92, with an extension to Glu100. Since this charged corridor largely coincides with the rotation axis (described above), its interactions with both ADP and ADP-BeFx actins are mainly preserved (Supplementary Video 1).

Another important charge interaction region at the actin and coronin interface in our model involves a cluster of actin residues Glu361, Asp363, and Glu364 and coronin arginines 361 and 362 (Fig. 3c). Actin’s Asp363 and Glu364 make contacts with two consecutive coronins along the same actin filament strand [or, *vice versa*, two different regions of the same coronin molecule contact the Asp363-Glu364 patch on two consecutive actin monomers in the same long-pitch strand (Fig. 3c)]. Specifically, Asp363 and Glu364 of “i” actin are in close proximity to coronin’s Arg141 and Lys142. Residues Glu361, Asp363, and Glu364 on the neighboring (“i+2”) actin are positioned close to the same coronin’s Arg361 and Arg362. This arrangement occurs in both nucleotide states of actin, albeit with different charge-charge interactions being coupled in each case, as described above (Fig. 3c, right).

Other noticeable interactions between coronin and actin in our model include Lys50 (on “i” actin’s D-loop), which interacts with a patch of negative charges on coronin around Asp273 (Fig. 3b). In addition, “i” actin’s Lys37 faces another patch of negative charges on coronin concentrated around Glu320 (Fig. 3b). The two patches are positioned similarly in both nucleotide state models; however the intrinsic flexibility of the D-loop, the presence of oppositely charged Asp51, and insufficient resolution of our structures make it difficult to compare accurately these regions in the two nucleotide states. Importantly, the C-terminus and the D-loop of actin are well recognized nucleotide state sensors of actin (reviewed in ref.[34]). We therefore speculate that the differences in coronin binding to ADP and ADP-BeFx actin originate from nucleotide-dependent conformational transitions in these areas.

We verified the importance of the interactions reported above via mutagenesis of actin and by determining the binding affinity of mutant ADP-actins for coronin (Table 1 and Supplementary Fig. 4 and 5). Based on our pseudo-atomic model of the coronin-actin complex, the lysine patch 204–207 on coronin plays a crucial role in actin binding. Indeed, mutating complementary residues on actin (Glu99 and Glu100) to alanines, caused the binding affinity of coronin for F-actin to decrease 18-fold compared to that of wild type

actin. Glu83-Asp84 and Asp363-Glu364 of actin are also critical for coronin's binding. Their substitution with alanines decreases the binding affinity of these mutants seven and five-fold, respectively. Interestingly, Asp363-Glu364 are located at the border between two consecutively bound coronin molecules, making it possible for this negative patch on actin to contribute to the binding of both coronins. Moreover, the sensitivity of actin's C-terminus to the nucleotide state argues for its role in the observed nucleotide-dependent interaction patterns of coronin and actin. In line with the results of the above actin mutations, mutants of complementary residues on coronin identified in this study (Arg141 and Lys142 in one positive patch and Arg361-Arg362 in another) were shown previously to affect severely coronin's binding to F-actin[25]. Other mapped interactions of coronin with actin contribute less to their binding energy, resulting in up to a 2-fold affinity decrease when the respective actin residues are mutated to alanine (Table 1).

As another approach to testing actin's charge interactions with coronin, we carried out their zero-length chemical crosslinking with 1-ethyl-3-(3-dimethylaminopropyl) carbodiimide (EDC)[35–37]. EDC can be used to activate acidic residues on actin, mainly at its N-terminus, and then covalently link them to amine groups in the bound protein[35–37]. We observed that EDC-activated α-skeletal actin filaments could be covalently crosslinked to coronin (Fig. 5a). The crosslinking may occur to the N-terminus of coronin. This is suggested by the proximity of actin's N-terminus in the cryoEM map (Fig. 5b) to the extra density that can be ascribed to the N-terminal residues of coronin (Fig. 5c). Interestingly, yeast coronin was crosslinked less efficiently to yeast actin than to α-skeletal rabbit actin (Fig. 5a). This was most likely because yeast actin's N-terminus contains only 2 negatively charged residues while α-actin's N-terminus contains four (Fig. 5). Indeed, when we used a yeast actin mutant with a neutralized N-terminus- D2N E4Q (DNEQ actin)[38] its EDC-activated crosslinking to coronin was the lowest (Fig. 5a). A minor amount of crosslinked actin-coronin complex formed with that actin mutant (Fig. 5a) could arise from EDC activation of actin residues E99-E100[39] and D363-E364[36,37]. Interestingly, DNEQ actin and yeast actin with its three N-terminal residues deleted (ΔDSE[38]) show less than 50% change in their binding affinity for coronin relative to WT actin (Table 1), indicating a low overall contribution of actin's N-terminus to coronin binding.

Discussion

Our structural analysis of coronin-actin complexes stems from our interest in deciphering coronin's role in assisting Arp2/3 complex-mediated actin branching and regulating the nucleotide-dependent severing of actin filaments by cofilin (reviewed in[12,13]). The initial step towards understanding the mechanism of such complex interactions and effects of coronin is to obtain a structural map of its complex with actin filaments in both the ADP and ADP-Pi (ADP-BeFx in this study) states.

Low resolution negative stain EM analysis of coronin-F-actin led to specific predictions of contact surfaces between these proteins[40]. However, mutational scanning of clusters of charged residues on coronin and assays of their effect on the affinity for actin suggested a set of different actin interaction sites on coronin[25]. The pseudo-atomic models of coronin-F-actin structures (in ADP- and ADP-BeFx-states) derived from our cryoEM data (Fig.1 and

Supplementary Fig. 2) are consistent with the loss of affinity for actin in coronin mutants[25]: Crn1-2 (K10A R12A), Crn1-6 (R141A K142A), Crn1-13 (K295A D297A), Crn1-17(E320A R323A), and Crn1-19(R361A R362A E364A E365A). All of these clusters are located at the coronin-actin interface proposed in the present study (Figs. 2, 3, Supplementary Fig. 4 and Supplementary Table 1). Our ADP-actin-coronin model suggests that the coronin residues identified by Ghandi and coworkers[25] make contacts with actin residues 37, 39, 50–51, 80–84 and 360–364 (Supplementary Table 1, Figs. 2 and 3). Indeed, our results (Table 1 and Supplementary Fig. 4) showed that ADP-actin filaments of R37A R39A, K50A D51A, D80A D81A, E83A D84A, and D363A E364A mutants had a ≥2-fold decrease in their binding affinity to coronin. The affinity decrease was greater when a mutation on actin impacted several corresponding binding sites on Crn1-ΔCC, for example D363A E364A (Supplementary Table 1). Notably, as predicted by our model of actin-coronin contacts, mutation of Glu99 and Glu100 had a large impact on coronin-actin binding (Table 1). The interest in this site is augmented by its contribution to the binding of several other actin binding proteins such as myosin[41–43], drebrin[44], actobindin[45], and even a glycolytic enzyme aldolase[46]. Conceivably, such interactivity of this site may be implicated in competitive compartmentalization of these, and perhaps other, F-actin binding proteins in various regions of the cell. Overall, both actin based mutagenesis and cryoEM based models are in agreement with the actin binding footprint on coronin identified by Gandhi et al.[25]. Obviously, the actin-coronin structure reported here is at higher resolution and more comprehensive than in previous models (Fig. 1).

Functional assays of coronin's effect on actin filament severing by cofilin indicate that coronin should not interfere with cofilin binding to ADP-actin, while even inhibiting its interaction with ATP-actin[13,17]. Our work provides structural explanation for the cooperation between cofilin and coronin. When we superimpose our models with the Galkin et al.'s high resolution cryoEM model of F-actin and human cofilin 2[24], there is partial clash of coronin and cofilin binding maps (Fig.6a and 6b, Supplementary Video 2) in the ADP-Pi state (simulated by the ADP-BeFx complex in this study). This suggests their binding competition, and offers explanation for coronin's protection of freshly polymerized filaments (mainly in the ADP-Pi state) from severing. Importantly, in the ADP state of F-actin the steric clash observed between blade 5 of coronin and the N-terminal helix of cofilin is released (Fig. 6c). Thus, as judged by the immediate proximity of the surfaces of coronin (this work) and cofilin[24] in the superimposed reconstructions (Fig. 6c), coronin would allow and/or promote cofilin binding, resulting in greater severing in the ADP state of F-actin[17,25]. Furthermore, because shearing of actin filaments by cofilin occurs mainly at the boundaries between cofilin decorated and undecorated segments[47], it is plausible that coronin may support the formation of such boundaries by reinforcing the bare actin-like conformation at the sites it occupies while also promoting adjacent binding of cofilin.

Next, to gain insight into the structural basis of concentration dependent inhibition and activation of Arp2/3 complex in the presence of coronin[12,16], we superimposed our actin-coronin models and the Arp2/3 complex-actin filament model[48]. The location of coronin on the mother filament overlaps with that of the Arp2/3 complex in both nucleotide models (Supplementary Fig. 6), as the footprints of coronin on actin "i" and "i+2" clash with ArpC3 and ArpC2/ArpC4, respectively. Therefore, at high coronin decorations, binding of the

Arp2/3 complex to F-actin would be inhibited in agreement with previous structural findings[48]. However, under non-saturating conditions, coronin and Arp2/3 complex can bind next to each other and even promote mutual recruitment to actin filaments. This is consistent with the reported coronin concentration-dependent switch of Arp2/3 complex's activity[12,16].

Nucleotide-based conformational rearrangements in both G- and F-actin are critical in modulating and controlling actin dynamics at the cellular level. Several areas on the actin subunit are recognized as primary and secondary conformational sensors. The primary sensors are located in direct proximity to the nucleotide binding cleft and transfer conformational changes from the nucleotide to peripheral sensors (reviewed in ref.[34]). The secondary sensors are peripherally located; they control nucleotide-dependent differential binding of regulatory proteins. Among the four well recognized peripheral sensory regions – the V-stretch (residues 227–237)[49], W-loop (residues 165–172)[50], D-loop (residues 40–51)[51,52], and C-terminus[53] – the latter two make prominent contacts with coronin and are likely to contribute to the observed nucleotide state differences. The D-loop is not well defined in our reconstructions and therefore its role in the observed transitions is speculative at this stage. On the other hand, the footprint of coronin binding to the C-terminal helix of actin (residues 350–364) clearly differs in the two nucleotide states, with more prominent contacts detected in the ADP-BeFx state (Fig. 2c,d). Mutations on actin that involve this region (Table 1) as well as the corresponding mutations on coronin[25], severely affect the affinity of these proteins for each other. Therefore, we may speculate that tighter binding of coronin to the C-terminus of i+2 actin in the ADP-BeFx state overrides the larger contact area between coronin and the i+1 actin subunit on the opposite strand of actin. The C-terminus of actin, which participates in the binding of two consecutive coronin molecules, is known to be allosterically coupled[53] to the D-loop, thereby adding indirect support for the role of these two areas in nucleotide-dependent regulation of coronin-actin interactions.

In conclusion, we provided intermediate resolution cryoEM images of the coronin-actin complex and predicted protein-protein contacts with high precision. We also presented specific nucleotide state differences in the structure of actin-coronin complexes. To the best of our knowledge, this is the first report of structural mapping of nucleotide state driven differences in actin-ABP complexes and the best resolution structures of such complexes. When combined with the previously reported structures of actin-cofilin and actin-Arp2/3 complex, our model offers structural explanation for coronin's regulation of cofilin and Arp2/3 complex interactions with ADP-actin and ADP-Pi-actin.

ONLINE METHODS

Purification of actin and Crn1ΔCC

Rabbit skeletal muscle α-actin was prepared according to Spudich and Watt[54] and kept in buffer A (5 mM Tris (pH 8.0), 0.5 mM β-mercaptoethanol, 0.2 mM ATP, and 0.2 mM $CaCl_2$). Baker's yeast and yeast actin mutant strains DNEQ[38], ΔDSE[38], R37A R39A[55], K50A D51A[56], D80A D81A[42], E83A D84A[42], E99A E100A[42], K315A E316A[57], and D363A E364A[55] were purified by DNase-I affinity chromatography[58]. Yeast actin was cycled after purification as previously described[58] and kept in buffer B (10 mM HEPES (pH 7.4), 1 mM dithiothreitol (DTT), 0.2 mM ATP, and 0.2 mM $CaCl_2$) on ice. Bacterial

expression plasmids for full length and GST-Crn1ΔCC (residues 1–600) were kindly provided by Dr. B. Goode's laboratory (Brandeis University)[25]. Coronin proteins were expressed in *E.coli* strain BL21 (DE3) and purified as described[25].

Preparation of coronin-actin complexes

Rabbit α-actin was dialyzed into buffer C (10 mM TRIS (pH7.5), 0.2 mM $CaCl_2$, 0.2 mM ATP and 1mM DTT). The resulting Ca-ATP-actin was exchanged to Mg-ATP-actin (with 50 μM $MgCl_2$ and 0.4mM EGTA) over 5 minutes. Following this, 20 μM Mg-ATP-actin was polymerized with 1mM $MgCl_2$ and 50 mM KCl for 15 minutes at room temperature and then kept on ice. ADP-BeFx-actin was prepared by incubating F-actin with 0.1 mM $BeCl_2$ and 5 mM NaF for 1–2 hour on ice. Coronin was dialyzed into buffer C containing 50 mM KCl. Samples for cryoEM were prepared by diluting ADP-BeFx-F-actin to 2 μM in the presence of 6–8 μM Crn1ΔCC (final concentration). ADP-F-actin was prepared from Mg-ATP-actin in buffer C with additional 0.3 mM ATP. After 30 minute polymerization at room temperature, 8 units/ml hexokinase and 1 mM dextrose was added to deplete the remaining ATP over 1 hour, on ice. Samples for cryoEM were later prepared by diluting the stock ADP-F-actin (20μM) to 2μM in the presence of 6–8 μM Crn1ΔCC using an F-buffer (buffer C with 1 mM $MgCl_2$ and 50 mM KCl and no ATP) supplemented with 0.5 mM ADP.

Cryo electron microscopy and refinement

An aliquot of sample was applied to Quatifoil 1.2/1.3 grids (actual hole size 1.6 μm). These grids were treated with ethylene-dichloride, coated with fresh carbon and baked under 100keV electron beam overnight[59]. The grid was then blotted and vitrified in liquid nitrogen cooled liquid ethane, in a vitrobot (FEI) machine. The vitrification parameters were: blot force 1, blot time 4s, blot once, wait time 2s, drain time 2s; sample volume applied to each grid was: 2.5 μL.

Each grid was loaded into FEI Titan Krios microscope with autoloader. The microscope was operated at 120kV. CryoEM images were recorded digitally with a Gatan ultrascan 16 mega-pixel CCD camera at 59,000× magnification. The calibrated pixel size is 1.437 Å. A total of 1380 and 1200 CCD frames have been recorded for ADP and ADP-BeFx states, respectively. The defocus values ranged from 2–4 μm.

Image quality was then evaluated by their Fourier transforms. Decorated actin filaments were selected manually with EMAN *helixboxer*[60]. A total of 883 and 348 images were used for the final reconstruction for ADP and ADP-BeFx states, respectively. Other images were rejected by evaluating Fourier spectra. The selected filaments were segmented into boxes by 88% overlap, giving 53,001 and 45,307 boxes (103,800 and 88,080 asymmetric units) for ADP and ADP-BeFx states, respectively. (Each box is 320×320 in dimensions, giving about 1¼ repeats of actin per box.) We then sorted each dataset against our early reconstructions of coronin decorated actin filaments in ADP and ADP-BeFx states and in undecorated actin filaments. In each dataset we kept the population that aligned best with the model corresponding to the desired state (the alignments are scored by EMAN with Fourier-ring correlation option.) Among the selected particles, we cut off those with EMAN alignment scores that were one or more standard deviations worse than average. The total numbers of

boxes used for reconstruction was 31,141 and 26,805 (60,720 and 52,260 asymmetric units) for ADP and ADP-BeFx states, respectively.

We then performed single particle based helical reconstruction on each set of these particles. We used EMAN–based IHRSR[61] to generate an initial reconstruction for each of the two states. The initial models were generated in a similar fashion as previous models[62]. We used a customized version of Relion[63] to do real-space helical reconstructions and finalize the refinement. This "helical" Relion contains an implementation of IHRSR methods based on Relion's software framework. We used the "Gold-standard" scheme to estimate our resolutions. The structures were refined with the "auto-refine" function of Relion until convergence.

Modeling of coronin decorated actin filaments

We built a homology model for yeast coronin 1 based on the crystal structure of mouse coronin 1a (PDB: 2aq5)[21], by SWISS-MODEL on Expasy server[64]. We docked this model and the pseudoatomic model of actin per subunit (PDB: 3mfp)[26] into the two structures by Chimera, using the "fit into map" function. Both models fit unambiguously the corresponding densities in both structures.

We visualized the interaction between coronin and actin in the two states in Chimera and PyMol (http://www.pymol.org/). The figures that contain cryoEM envelopes and pseudoatomic structural models were rendered by Chimera[65].

Fluorescence spectroscopy

Rabbit α-actin was labelled with acrylodan at Cys374 as previously described[56]. DTT-free Ca-G-actin was incubated with a 2-fold mole excess of acrylodan for 2.5 hr, at 24°C. The labelling reactions were quenched with 1 mM DTT followed by the removal of excess acrylodan on a G-50 Sephadex column. ADP-F- and ADP-BeFx-F-actin samples were prepared from labelled actin as described above. Fluorescence emission spectra of labelled ADP-F-actin and ADP-BeFx-F-actin in the absence and presence of Crn1ΔCC were recorded between 400–650 nm, with the excitation wavelength set at 385 nm, using a PTI (Photon Technology International) spectrofluorometer. Figures 2e and 2f show representative spectra obtained in experiments yielding identical results (two repeats).

Cosedimentation Experiments

Cosedimentation experiments were done as previously reported[25] with minor modifications. Crn1ΔCC (1.0 μm) was incubated with increasing concentrations (0–30 μm) of polymerized wild type and mutant yeast actins for 15 min and then centrifuged for 25 min at 90,000 rpm in a Beckman TLA100 rotor. Pellets and supernatants were run on SDS-PAGE and the percentage of coronin bound to actin was calculated by densitometry analysis of the corresponding bands on Coomassie-stained gels using Scion Image. The binding curves were obtained using Systat SigmaPlot for each of the independent repeats (mostly three). Representative binding curves are shown in Supplemental Fig. 3.

Zero length crosslinking with EDC/NHS

EDC/NHS (Thermo Scientific-Pierce Biotechnology) crosslinking of F-actin and Crn1ΔCC was done according to a two-step reaction protocol[66] in the manufacturer's instructions. In short, α-skeletal, WT-, and DNEQ actins were exchanged into 5 mM MES (pH 6.0) buffer supplemented with 0.2 mM ATP and 0.2 mM $CaCl_2$ using G-50 desalting columns. 15 μM aliquots of these actins were polymerized as described above. After F-actins were activated with 15 μM EDC and 15μM Sulfo-NHS (for 15 minutes at 24°C), excess reagents were quenched with 0.5 mM BME. Crn1ΔCC and NHS-ester activated F-actins were mixed to a final concentration of 10 μM each, and the pH of the solution was raised above pH 7.0 (using 1M HEPES buffer at pH7.6) to initiate crosslinking reactions. Reaction aliquots were taken at different time intervals and run on SDS-PAGEs.

Supplementary Material

Refer to Web version on PubMed Central for supplementary material.

Acknowledgments

This work was supported by US National Institutes of Health (US NIH) grants GM077190 (to E.R.), GM071940 and AI094386 (to Z.H.Z.), F32HL119069 (to Z.A.O.D.), American Heart Association postdoctoral fellowship 13POST17340020 (to P.G.), and a start up fund from The Ohio State University (to D.S.K). The authors acknowledge the use of instruments at the Electron Imaging Center for NanoMachines supported by US NIH grant 1S10RR23057 (to Z.H.Z.) and CNSI at UCLA. The authors acknowledge also the use of computer time at The Extreme Science and Engineering Discovery Environment (XSEDE) resources (MCB130126 to Z.H.Z.). The content is solely the responsibility of the authors and does not necessarily represent the official views of the National Institutes of Health.

References

1. Orlova A, Egelman EH. Structural basis for the destabilization of F-actin by phosphate release following ATP hydrolysis. J Mol Biol. 1992; 227:1043–1053. [PubMed: 1433285]
2. Isambert H, et al. Flexibility of actin filaments derived from thermal fluctuations. Effect of bound nucleotide, phalloidin, and muscle regulatory proteins. J Biol Chem. 1995; 270:11437–11444. [PubMed: 7744781]
3. Orlova A, Egelman EH. A conformational change in the actin subunit can change the flexibility of the actin filament. J Mol Biol. 1993; 232:334–341. [PubMed: 8345515]
4. Fujiwara I, Vavylonis D, Pollard TD. Polymerization kinetics of ADP- and ADP-Pi-actin determined by fluorescence microscopy. Proceedings of the National Academy of Sciences of the United States of America. 2007; 104:8827–8832. [PubMed: 17517656]
5. Khaitlina SY, Strzelecka-Golaszewska H. Role of the DNase-I-binding loop in dynamic properties of actin filament. Biophys J. 2002; 82:321–334. [PubMed: 11751319]
6. Muhlrad A, Cheung P, Phan BC, Miller C, Reisler E. Dynamic properties of actin. Structural changes induced by beryllium fluoride. J Biol Chem. 1994; 269:11852–11858. [PubMed: 8163484]
7. Bamburg JR, McGough A, Ono S. Putting a new twist on actin: ADF/cofilins modulate actin dynamics. Trends Cell Biol. 1999; 9:364–370. [PubMed: 10461190]
8. Andrianantoandro E, Pollard TD. Mechanism of actin filament turnover by severing and nucleation at different concentrations of ADF/cofilin. Molecular cell. 2006; 24:13–23. [PubMed: 17018289]
9. Suarez C, et al. Cofilin tunes the nucleotide state of actin filaments and severs at bare and decorated segment boundaries. Current biology : CB. 2011; 21:862–868. [PubMed: 21530260]
10. Blanchoin L, Pollard TD, Mullins RD. Interactions of ADF/cofilin, Arp2/3 complex, capping protein and profilin in remodeling of branched actin filament networks. Current biology : CB. 2000; 10:1273–1282. [PubMed: 11069108]

11. Pollard TD, Borisy GG. Cellular motility driven by assembly and disassembly of actin filaments. Cell. 2003; 112:453–465. [PubMed: 12600310]
12. Chan KT, Creed SJ, Bear JE. Unraveling the enigma: progress towards understanding the coronin family of actin regulators. Trends Cell Biol. 2011; 21:481–488. [PubMed: 21632254]
13. Gandhi M, Goode BL. Coronin: the double-edged sword of actin dynamics. Subcell Biochem. 2008; 48:72–87. [PubMed: 18925372]
14. Cai L, Makhov AM, Bear JE. F-actin binding is essential for coronin 1B function in vivo. J Cell Sci. 2007; 120:1779–1790. [PubMed: 17456547]
15. Humphries CL, et al. Direct regulation of Arp2/3 complex activity and function by the actin binding protein coronin. J Cell Biol. 2002; 159:993–1004. [PubMed: 12499356]
16. Liu SL, Needham KM, May JR, Nolen BJ. Mechanism of a concentration-dependent switch between activation and inhibition of Arp2/3 complex by coronin. Journal of Biological Chemistry. 2011; 286:17039–17046. [PubMed: 21454476]
17. Gandhi M, Achard V, Blanchoin L, Goode BL. Coronin switches roles in actin disassembly depending on the nucleotide state of actin. Mol Cell. 2009; 34:364–374. [PubMed: 19450534]
18. Mueller P, et al. Regulation of T cell survival through coronin-1-mediated generation of inositol-1,4,5-trisphosphate and calcium mobilization after T cell receptor triggering. Nat Immunol. 2008; 9:424–431. [PubMed: 18345003]
19. Shiow LR, et al. Severe combined immunodeficiency (SCID) and attention deficit hyperactivity disorder (ADHD) associated with a Coronin-1A mutation and a chromosome 16p11.2 deletion. Clin Immunol. 2009; 131:24–30. [PubMed: 19097825]
20. Shiow LR, et al. The actin regulator coronin 1A is mutant in a thymic egress-deficient mouse strain and in a patient with severe combined immunodeficiency. Nat Immunol. 2008; 9:1307–1315. [PubMed: 18836449]
21. Appleton BA, Wu P, Wiesmann C. The crystal structure of murine coronin-1: a regulator of actin cytoskeletal dynamics in lymphocytes. Structure. 2006; 14:87–96. [PubMed: 16407068]
22. McArdle B, Hofmann A. Coronin structure and implications. Subcell Biochem. 2008; 48:56–71. [PubMed: 18925371]
23. Goode BL, et al. Coronin promotes the rapid assembly and cross-linking of actin filaments and may link the actin and microtubule cytoskeletons in yeast. J Cell Biol. 1999; 144:83–98. [PubMed: 9885246]
24. Galkin VE, et al. Remodeling of actin filaments by ADF/cofilin proteins. Proc Natl Acad Sci U S A. 2011; 108:20568–20572. [PubMed: 22158895]
25. Gandhi M, Jangi M, Goode BL. Functional surfaces on the actin-binding protein coronin revealed by systematic mutagenesis. J Biol Chem. 2010; 285:34899–34908. [PubMed: 20813846]
26. Fujii T, Iwane AH, Yanagida T, Namba K. Direct visualization of secondary structures of F-actin by electron cryomicroscopy. Nature. 2010; 467:724–728. [PubMed: 20844487]
27. Murakami K, et al. Structural basis for actin assembly, activation of ATP hydrolysis, and delayed phosphate release. Cell. 2010; 143:275–287. [PubMed: 20946985]
28. Fisher AJ, et al. Structural studies of myosin:nucleotide complexes: a revised model for the molecular basis of muscle contraction. Biophys J. 1995; 68:19S–26S. discussion 27S–28S. [PubMed: 7787065]
29. Fisher AJ, et al. X-ray structures of the myosin motor domain of Dictyostelium discoideum complexed with MgADP.BeFx and MgADP.AlF4. Biochemistry. 1995; 34:8960–8972. [PubMed: 7619795]
30. Combeau C, Carlier MF. Probing the mechanism of ATP hydrolysis on F-actin using vanadate and the structural analogs of phosphate BeF-3 and A1F-4. The Journal of biological chemistry. 1988; 263:17429–17436. [PubMed: 3182855]
31. Malm B, Larsson H, Lindberg U. The profilin--actin complex: further characterization of profilin and studies on the stability of the complex. J Muscle Res Cell Motil. 1983; 4:569–588. [PubMed: 6643679]
32. Duong AM, Reisler E. C-terminus on actin: spectroscopic and immunochemical examination of its role in actomyosin interactions. Adv Exp Med Biol. 1994; 358:59–70. [PubMed: 7801812]

33. Crosbie RH, Chalovich JM, Reisler E. Interaction of caldesmon and myosin subfragment 1 with the C-terminus of actin. Biochem Biophys Res Commun. 1992; 184:239–245. [PubMed: 1567431]
34. Kudryashov DS, Reisler E. ATP and ADP actin states. Biopolymers. 2013; 99:245–256. [PubMed: 23348672]
35. Chen T, Applegate D, Reisler E. Cross-linking of actin to myosin subfragment 1 in the presence of nucleotides. Biochemistry. 1985; 24:5620–5625. [PubMed: 3878158]
36. Andreev OA, Saraswat LD, Lowey S, Slaughter C, Borejdo J. Interaction of the N-terminus of chicken skeletal essential light chain 1 with F-actin. Biochemistry. 1999; 38:2480–2485. [PubMed: 10029542]
37. Sutoh K. Identification of myosin-binding sites on the actin sequence. Biochemistry. 1982; 21:3654–3661. [PubMed: 7115691]
38. Crosbie RH, Miller C, Chalovich JM, Rubenstein PA, Reisler E. Caldesmon, N-terminal yeast actin mutants, and the regulation of actomyosin interactions. Biochemistry. 1994; 33:3210–3216. [PubMed: 8136356]
39. Grintsevich EE, et al. Mapping of drebrin binding site on F-actin. J Mol Biol. 2010; 398:542–554. [PubMed: 20347847]
40. Galkin VE, et al. Coronin-1A stabilizes F-actin by bridging adjacent actin protomers and stapling opposite strands of the actin filament. J Mol Biol. 2008; 376:607–613. [PubMed: 18177666]
41. Johara M, et al. Charge-reversion mutagenesis of Dictyostelium actin to map the surface recognized by myosin during ATP-driven sliding motion. Proceedings of the National Academy of Sciences of the United States of America. 1993; 90:2127–2131. [PubMed: 8460118]
42. Miller CJ, Reisler E. Role of charged amino acid pairs in subdomain-1 of actin in interactions with myosin. Biochemistry. 1995; 34:2694–2700. [PubMed: 7873552]
43. Katoh T, Morita F. Mapping myosin-binding sites on actin probed by peptides that inhibit actomyosin interaction. Journal of biochemistry. 1996; 120:580–586. [PubMed: 8902624]
44. Grintsevich EE, et al. Mapping of drebrin binding site on F-actin. Journal of molecular biology. 2010; 398:542–554. [PubMed: 20347847]
45. Vancompernolle K, Vandekerckhove J, Bubb MR, Korn ED. The interfaces of actin and Acanthamoeba actobindin. Identification of a new actin-binding motif. Journal of Biological Chemistry. 1991; 266:15427–15431. [PubMed: 1869561]
46. Ouporov IV, Knull HR, Thomasson KA. Brownian dynamics simulations of interactions between aldolase and G- or F-actin. Biophysical journal. 1999; 76:17–27. [PubMed: 9876119]
47. Suarez C, et al. Cofilin tunes the nucleotide state of actin filaments and severs at bare and decorated segment boundaries. Curr Biol. 2011; 21:862–868. [PubMed: 21530260]
48. Rouiller I, et al. The structural basis of actin filament branching by the Arp2/3 complex. J Cell Biol. 2008; 180:887–895. [PubMed: 18316411]
49. Splettstoesser T, Holmes KC, Noe F, Smith JC. Structural modeling and molecular dynamics simulation of the actin filament. Proteins. 2011; 79:2033–2043. [PubMed: 21557314]
50. Kudryashov DS, Grintsevich EE, Rubenstein PA, Reisler E. A nucleotide state-sensing region on actin. The Journal of biological chemistry. 2010; 285:25591–25601. [PubMed: 20530485]
51. Otterbein LR, Graceffa P, Dominguez R. The crystal structure of uncomplexed actin in the ADP state. Science. 2001; 293:708–711. [PubMed: 11474115]
52. Zheng X, Diraviyam K, Sept D. Nucleotide effects on the structure and dynamics of actin. Biophysical journal. 2007; 93:1277–1283. [PubMed: 17526584]
53. Strzelecka-Golaszewska H, Mossakowska M, Wozniak A, Moraczewska J, Nakayama H. Long-range conformational effects of proteolytic removal of the last three residues of actin. The Biochemical journal. 1995; 307(Pt 2):527–534. [PubMed: 7733893]
54. Spudich JA, Watt S. The regulation of rabbit skeletal muscle contraction. I. Biochemical studies of the interaction of the tropomyosin-troponin complex with actin and the proteolytic fragments of myosin. J Biol Chem. 1971; 246:4866–4871. [PubMed: 4254541]
55. Wertman KF, Drubin DG, Botstein D. Systematic mutational analysis of the yeast ACT1 gene. Genetics. 1992; 132:337–350. [PubMed: 1427032]

56. Oztug Durer ZA, Kamal JK, Benchaar S, Chance MR, Reisler E. Myosin binding surface on actin probed by hydroxyl radical footprinting and site-directed labels. J Mol Biol. 2011; 414:204–216. [PubMed: 21986200]
57. Korman VL, Tobacman LS. Mutations in actin subdomain 3 that impair thin filament regulation by troponin and tropomyosin. J Biol Chem. 1999; 274:22191–22196. [PubMed: 10428784]
58. Durer ZA, et al. Structural states and dynamics of the D-loop in actin. Biophys J. 2012; 103:930–939. [PubMed: 23009842]
59. Ge P, Poweleit N, Gunsalus RP, Zhou ZH. Deriving de novo atomic models by cryo electron microscopy. Journal of Visual Experiments. 2014 in press.
60. Ludtke SJ, Baldwin PR, Chiu W. EMAN: Semi-automated software for high resolution single particle reconstructions. Journal of Structural Biology. 1999; 128:82–97. [PubMed: 10600563]
61. Ge P, Zhou ZH. Hydrogen-bonding networks and RNA bases revealed by cryo electron microscopy suggest a triggering mechanism for calcium switches. Proceedings of the National Academy of Sciences of the United States of America. 2011; 108:9637–9642. [PubMed: 21586634]
62. Ge P, et al. Cryo-EM model of the bullet-shaped vesicular stomatitis virus. Science. 2010; 327:689–693. [PubMed: 20133572]
63. Scheres SHW. RELION: Implementation of a Bayesian approach to cryo-EM structure determination. Journal of Structural Biology. 2012; 180:519–530. [PubMed: 23000701]
64. Arnold K, Bordoli L, Kopp J, Schwede T. The SWISS-MODEL workspace: a web-based environment for protein structure homology modelling. Bioinformatics. 2006; 22:195–201. [PubMed: 16301204]
65. Pettersen EF, et al. UCSF Chimera--a visualization system for exploratory research and analysis. J Comput Chem. 2004; 25:1605–1612. [PubMed: 15264254]
66. Grabarek Z, Gergely J. Zero-length crosslinking procedure with the use of active esters. Anal Biochem. 1990; 185:131–135. [PubMed: 2344038]

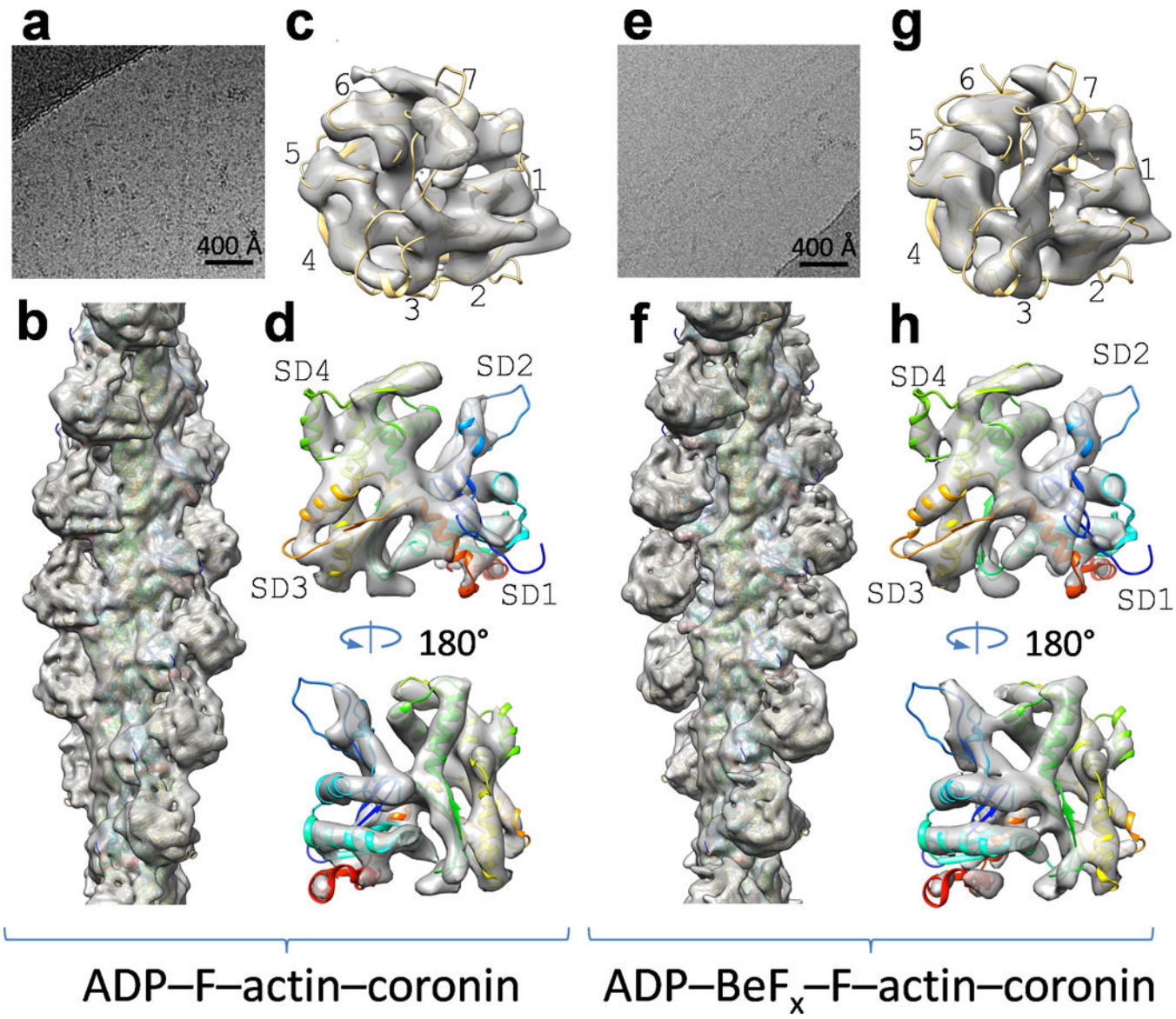

Figure 1. CryoEM reconstruction of coronin decorated actin filaments in both ADP and ADP-BeFx states

(**a–d**) ADP state. (**e–h**) ADP-BeFx state. (**a** and **e**) Areas of original images. (**b** and **f**) CryoEM reconstruction of coronin (Crn1ΔCC) decorated actin filaments (grey envelope) with an atomic model of actin and our homology model of coronin fitted (ribbons; actin: rainbow colors, coronin: gold; see text). (**c** and **g**) Densities corresponding to coronin (grey envelope) alone fitted with its atomic model (ribbon). 1–7 indicate the indexes of the blades of the propeller. (**d** and **h**) Densities corresponding to actin (grey envelope) alone fitted with its atomic model (ribbon). SD: subdomain.

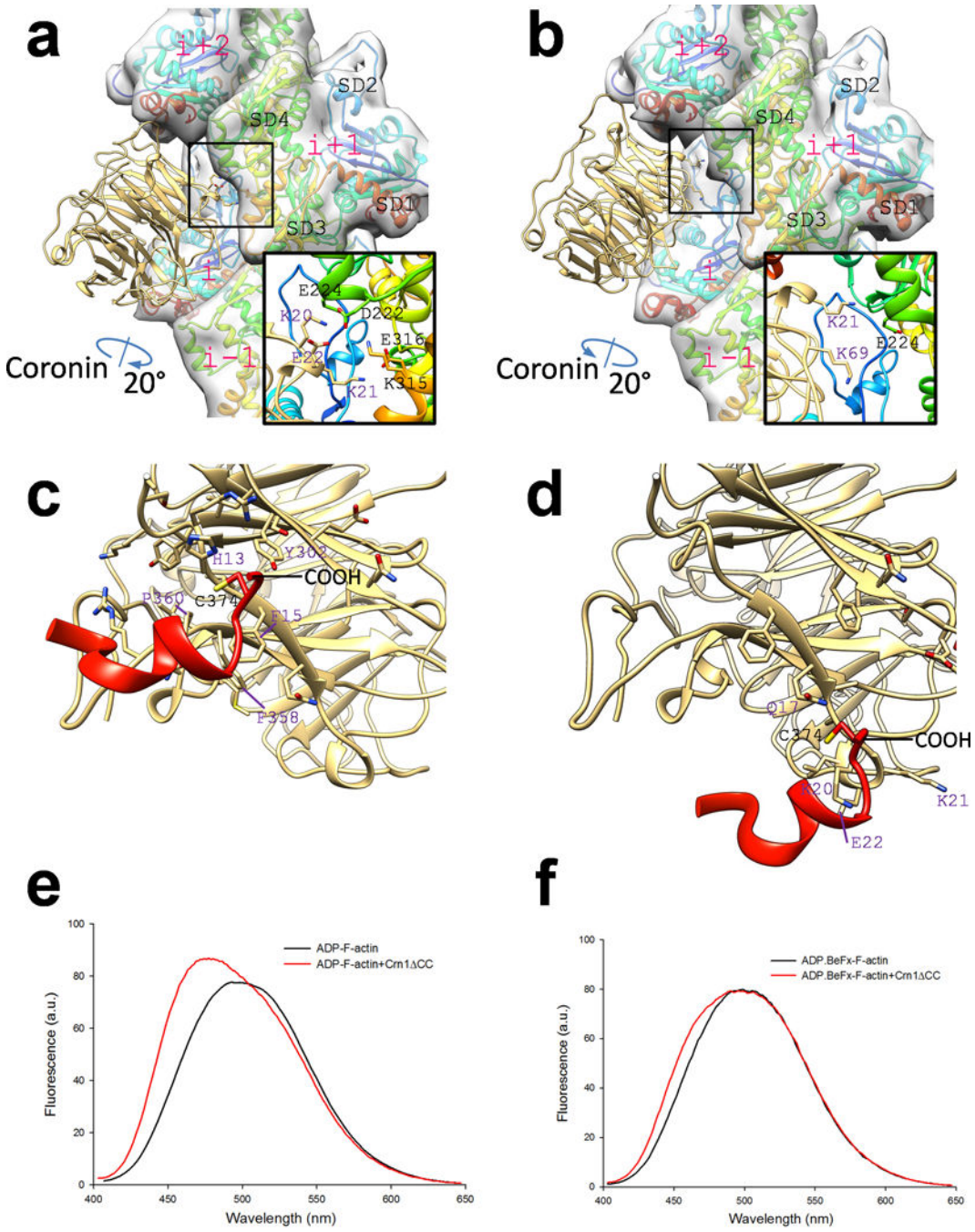

Figure 2. Different interaction modes between coronin and actin in ADP and ADP-BeFx states

(**a–d**) Pseudo-atomic models obtained by fitting an atomic model of actin and our homology model of coronin into our cryoEM densities (see text). (**a** and **b**) Differences in the overall binding modes between coronin and actin in ADP (**a**) and ADP-BeFx (**b**) states. Actin is shown in ribbons colored by rainbow colors (N-terminal: blue, C-terminal: red), with each subunit delineated with its grey transparent surface that is derived from its atomic model; coronin is shown in gold ribbons. Key interacting amino acids between coronin and actin i +1 are shown in sticks and are highlighted in insets. (**c** and **d**) Different environments of

Cys374 in ADP (**c**) and ADP-BeFx (**d**) states. Actin's C-terminal loop 371–375 is in red; the C-terminus marked by "COOH". (**e**) Fluorescence emission spectra of actin labeled with acrylodan at residue 374 in the ADP-actin-coronin complex and (**f**) the ADP-BeFx-actin-coronin complex. In panels (**a–d**), key residues are marked with labels of their single letter codes and residue numbers and are colored in black and purple for actin and coronin, respectively.

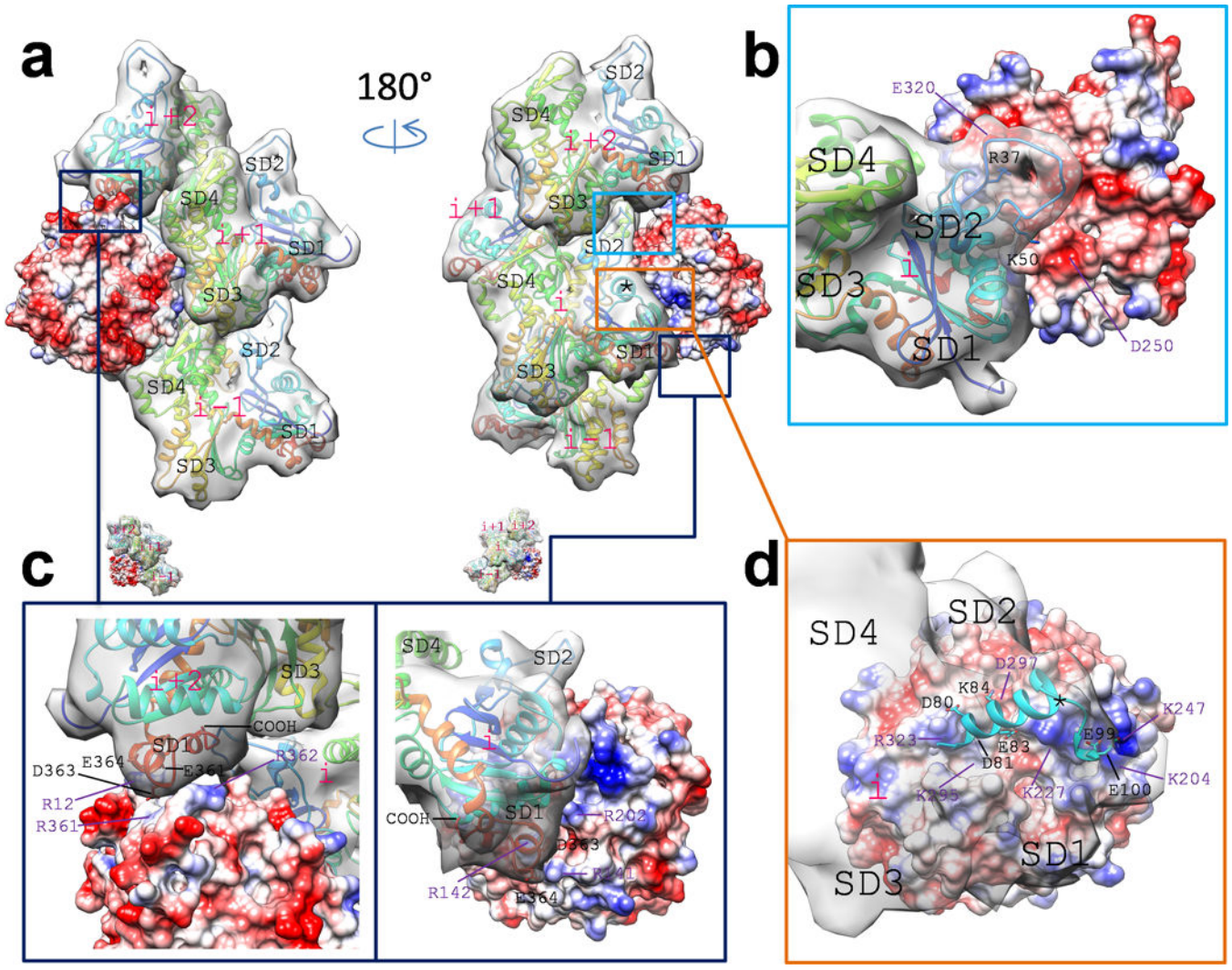

Figure 3. Interactions between coronin and filamentous actin in ADP state

(**a–d**) Pseudo-atomic models obtained by fitting an atomic model of actin and our homology model of coronin into cryoEM densities (see text). (**a**) Overview of actin-coronin interaction. One coronin subunit (red, white and blue surface) and its four neighboring actin subunits (grey surfaces with rainbow-colored ribbons) are shown from front and back. SD: subdomain. “i” indicates the actin subunit that most intensively interacts with this coronin subunit. “i+1”, “i+2” and “i−1” mark the relative position of adjacent actin subunits in the filament. Key interactions are boxed in this panel and highlighted in connected panels. In all panels, actin subunits are delineated by grey transparent surfaces derived from their atomic models. (**b**) Interaction between the D-loop of actin and coronin. Residues Arg37 and Lys50 face negatively charged patch on coronin. In all panels, key residues are marked with labels of their single letter codes and residue numbers, colored in black and purple for actin and coronin, respectively. (**c**) Interaction between actin’s C-terminal (COOH) helices (red ribbons in actin model) and coronin. Left, interaction between coronin and actin i+2; right, interaction between coronin and actin i. (**d**) The most critical charge interactions between coronin and actin are concentrated on actin’s helix 79–93 (star on panels **a** and **d**) with

extension to amino acid 100 (for clarity, residues 78–100 are shown exclusively in cyan ribbon, with key amino acids shown as sticks).

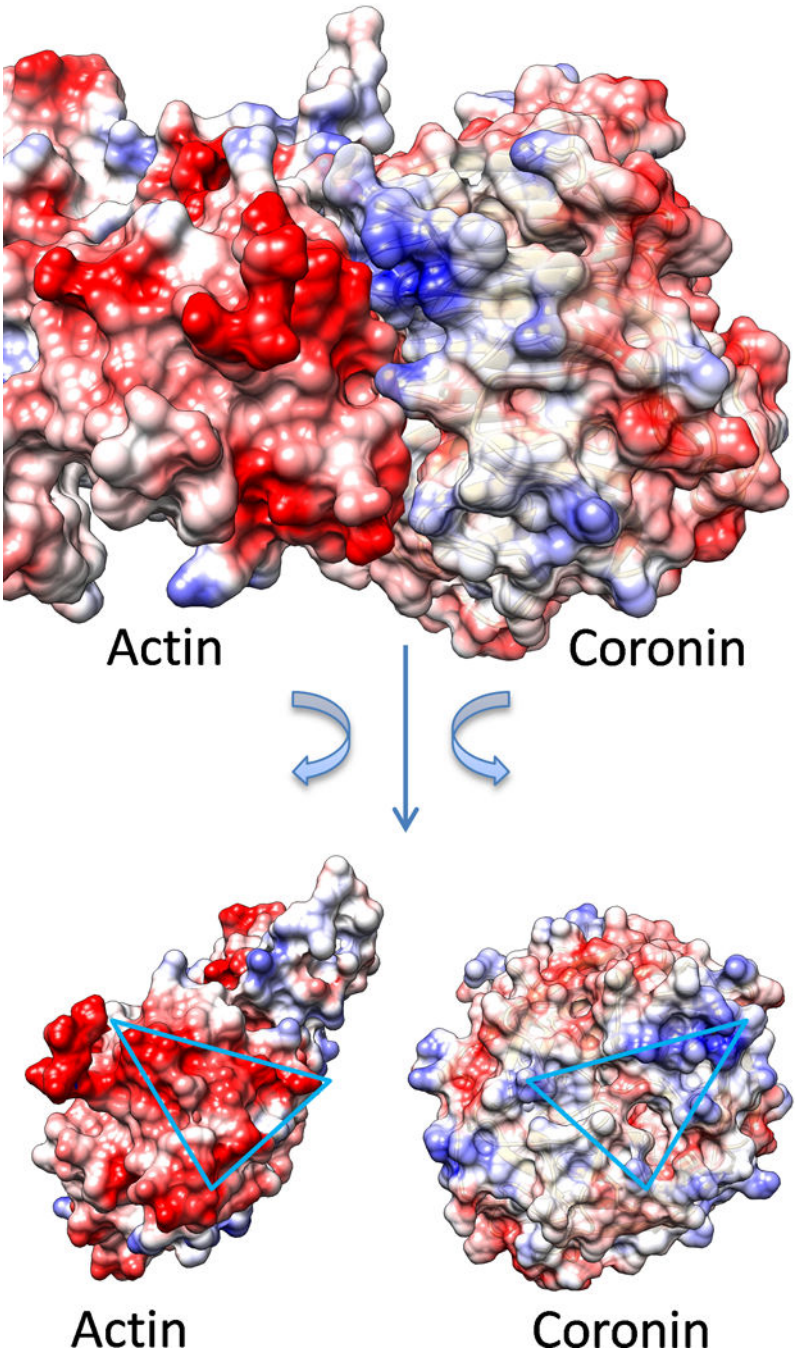

Figure 4. Charge and shape complementarity between actin and coronin

Pseudo-atomic models obtained by fitting an atomic model of actin and our homology model of coronin into our cryoEM densities (see text). Top, the pseudo-atomic model of actin-coronin complex is shown in molecular surface colored by surface charge. The surface for coronin (right) is semi-transparent, showing the ribbon model of coronin. Bottom, the interface between actin and coronin is shown in open-book configuration by turning each interacting surface 90° towards the page. The charged interactions between the two are concentrated in a triangular shape (blue).

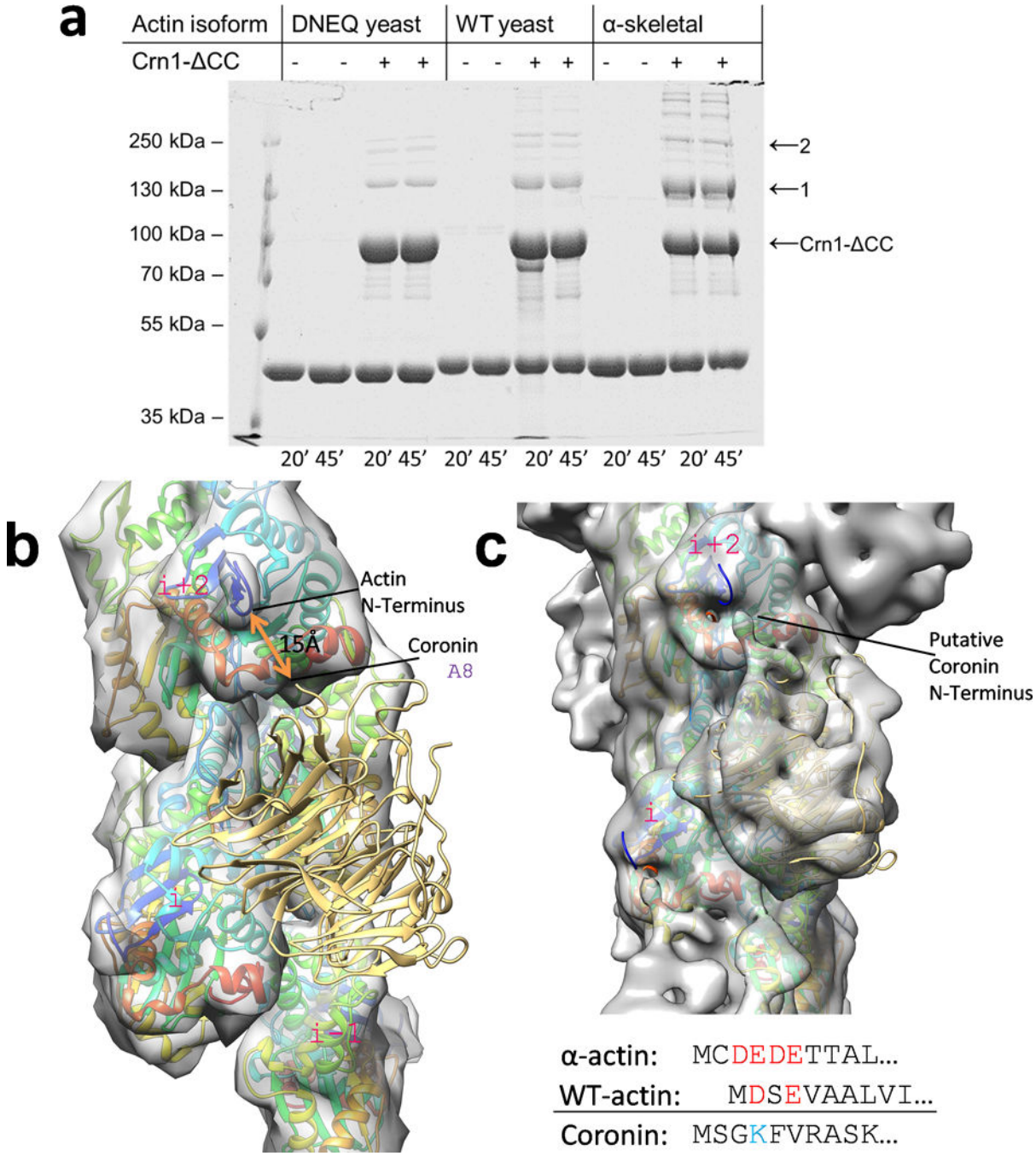

Figure 5. Crn1ΔCC and ADP-F-actin are crosslinked by EDC mainly, but not only, through actin's N-terminus

(**a**) SDS-PAGE analysis of actin-coronin EDC crosslinking. EDC activated α-skeletal (α-), wild type yeast (WT-), and DNEQ- F-actins were crosslinked with equimolar amounts of Crn1ΔCC for 20 or 45 minutes and then analyzed by SDS-PAGE. (1) indicates one actin in a complex with one coronin molecule. (2) indicates a protein complex involving more than one actin per coronin molecule. (**b**) Side view of the pseudo-atomic model of the actin-coronin complex showing proximity of the N-termini of actin (ribbons in rainbow colors

with grey transparent surfaces derived from its atomic model) and coronin (gold ribbons). (**c**) Patch of density attributed to the N-terminal residues of coronin extends from coronin towards the N-terminus of actin. N-terminal amino acid sequences are given for α-skeletal actin, WT yeast actin and coronin. Charged residues that are most likely involved in EDC crosslinking are highlighted in blue and red.

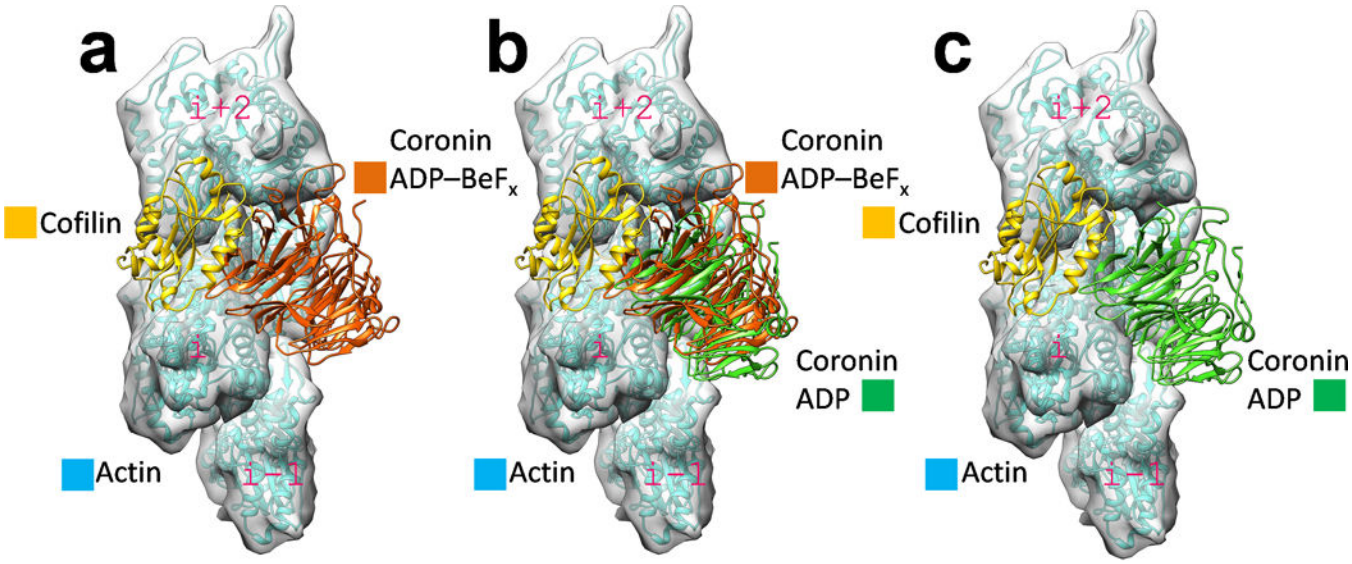

Figure 6. Modeling of cofilin on the coronin decorated F-actin in ADP-BeFx and ADP states

(a) The pseudo-atomic models of actin-coronin in ADP-BeFx state and actin-cofilin are superimposed by aligning actin i. For clarity, actin subunits are shown for the actin-coronin complex in ADP state only and are delineated by grey transparent surfaces derived from its atomic model. (**b**) For comparison, the pseudo-atomic model of actin-coronin in ADP state is superimposed on the previous model in a similar way. (**c**) A separate model that includes only actin-coronin in ADP state and cofilin superimposed as in (**a**). A noticeable main chain clash between coronin and cofilin can be seen in the ADP-BeFx state (**a**) but not in the ADP state (**c**).

Table 1

Summary of Crn1-DCC binding affinities for WT and mutant yeast actins

	Kd (μM)	Kd/Kd_{WT}	Coronin residues in close proximity
WT	0.87 ± 0.04	1.00	
DNEQ*	0.81 ± 0.01	~ 1	
ΔDSE**	0.76 ± 0.03	~1	
K50A/D51A (red***)	1.55 ± 0.06	~2	D250 and D273
D80A/D81A (magenta)	1.9 ± 0.5	~2	R323, K295
E83A/K84A (blue)	5.8 ± 0.3	~7	K227, D297
E99A/E100A (cyan)	16	~18	K204, K247
K315A/E316A (green)	1.4 ± 0.1	~1.6	K20, K21 and E22 (with actin “i+1”)
D363A/E364A (yellow)	4.4 ± 0.8	~5	R141, R142, and R202 (with actin “i”) R361 and R362 (with actin “i +2”)
R37A/R39A (orange) +Phalloidin ****	2.7 ± 0.1	~3	E320
WT+150 mM KCl	2.3	~2–3	

* - D2N/E4Q actin mutant with a neutralized N-terminus.

** ΔDSE – mutant actin with its three N-terminal residues deleted

*** Color names in parentheses refer to the colors of these residues in Supplementary Fig. 5

**** This set of measurement was carried out in the presence of equimolar concentrations of phalloidin.